Article

Molecular Cell

Nucleosome Turnover Regulates Histone Methylation Patterns over the Genome

Graphical Abstract

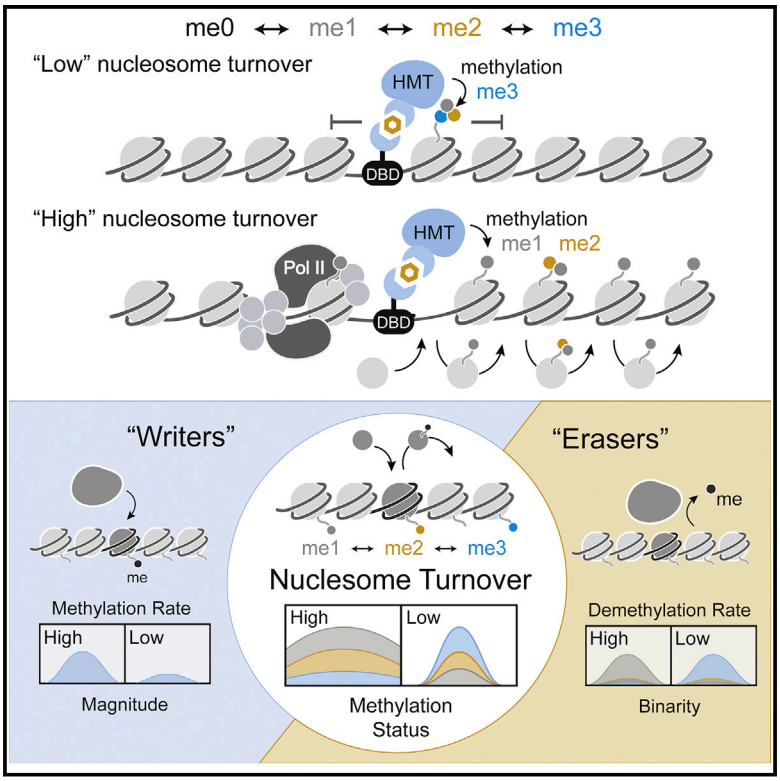

Highlights

- Chemical-induced proximity of DOT1L leads to ordered addition of H3K79me1, me2, and me3
- Methylation kinetics are loci specific and related to the rate of nucleosome turnover
- Genome-wide analyses reveal quantitative relationship between turnover/demethylation
- Simulations of turnover predict valence and topology of various histone modifications

Authors

Emma J. Chory, Joseph P. Calarco, Nathaniel A. Hathaway, Oliver Bell, Dana S. Neel, Gerald R. Crabtree

Correspondence

crabtree@stanford.edu

In Brief

Previous work has revealed that "writers" and "erasers" of histone modifications play a critical role in regulating gene expression. Now, studies by Chory et al. reveal that, in addition, the patterns, kinetics, and topology of histone modifications over the genome can be shaped by the rate of nucleosome turnover.

Chory et al., 2019, Molecular Cell *73*, 1–12
January 3, 2019
https://doi.org/10.1016/j.molcel.2018.10.028

CellPress

Please cite this article in press as: Chory et al., Nucleosome Turnover Regulates Histone Methylation Patterns over the Genome, Molecular Cell (2018), https://doi.org/10.1016/j.molcel.2018.10.028

Molecular Cell
Article

Nucleosome Turnover Regulates Histone Methylation Patterns over the Genome

Emma J. Chory,[1,2] Joseph P. Calarco,[2] Nathaniel A. Hathaway,[3] Oliver Bell,[4,5] Dana S. Neel,[2] and Gerald R. Crabtree[2,6,7,*]
[1]Department of Chemical Engineering, Stanford University, Stanford, CA 94305, USA
[2]Departments of Pathology and Developmental Biology, Stanford University School of Medicine, Stanford, CA 94305, USA
[3]Division of Chemical Biology and Medicinal Chemistry, Center for Integrative Chemical Biology and Drug Discovery, UNC Eshelman School of Pharmacy, Chapel Hill, NC 27599, USA
[4]Institute of Molecular Biotechnology of the Austrian Academy of Sciences (IMBA), Vienna Biocenter (VBC), 1030 Vienna, Austria
[5]Department of Biochemistry and Molecular Medicine and the Norris Comprehensive Cancer Center, Keck School of Medicine of the University of Southern California, Los Angeles, CA 90089-9601, USA
[6]Howard Hughes Medical Institute, Chevy Chase, MD, USA
[7]Lead Contact
*Correspondence: crabtree@stanford.edu
https://doi.org/10.1016/j.molcel.2018.10.028

SUMMARY

Recent studies have indicated that nucleosome turnover is rapid, occurring several times per cell cycle. To access the effect of nucleosome turnover on the epigenetic landscape, we investigated H3K79 methylation, which is produced by a single methyltransferase (Dot1l) with no known demethylase. Using chemical-induced proximity (CIP), we find that the valency of H3K79 methylation (mono-, di-, and tri-) is determined by nucleosome turnover rates. Furthermore, propagation of this mark is predicted by nucleosome turnover simulations over the genome and accounts for the asymmetric distribution of H3K79me toward the transcriptional unit. More broadly, a meta-analysis of other conserved histone modifications demonstrates that nucleosome turnover models predict both valency and chromosomal propagation of methylation marks. Based on data from worms, flies, and mice, we propose that the turnover of modified nucleosomes is a general means of propagation of epigenetic marks and a determinant of methylation valence.

INTRODUCTION

The histone methylation state of the epigenome is established through antagonizing enzymatic processes of "writing" and "erasing" histone modifications (Jenuwein and Allis, 2001). The formation and removal of covalent histone modifications occur in concert with nucleosome turnover that could conceivably alter the epigenetic landscape (Taneja et al., 2017). Despite the fact that histone modifications are indicative of stable epigenetic states, nucleosomes are exchanged several times within each cell cycle (Deal et al., 2010; Dion et al., 2007; Radman-Livaja et al., 2011), suggesting that histone modifications are rapidly erased by nucleosome turnover. These observations raise the question of how an epigenetic state is stably maintained in the face of continual nucleosome exchange. To study the role of nucleosome turnover in regulating histone modifications, we elected to first look at methylation of lysine 79 on histone 3 (H3K79), which is catalyzed by the multi-subunit disruptor of telomeric silencing (DOT1 methyltransferase), discovered in yeast (Singer et al., 1998). In mammals, a single gene encodes the K79 methyltransferase (DOT1L), yet importantly, there is no known dedicated histone demethylase that removes this mark. Despite being evolutionarily conserved and implicated in the development of mixed lineage leukemia (MLL) (Krivtsov and Armstrong, 2007), regulation by the DOT1L remains poorly understood. Mono-, di-, and tri-H3K79 methylation marks (me1, me2, and me3) are solely deposited by the DOT1L methyltransferase (Nguyen and Zhang, 2011), which is localized to unmodified H3K27 sites through a direct interaction with AF10/AF17 (Chen et al., 2015; Figure 1A). Furthermore, DOT1L is recruited specifically to active sites of the genome through binding of AF9 with acetylated H3K9 (H3K9Ac) (Li et al., 2014). Subunits of the DOT complex are commonly translocated in recurrent MLL-rearranged leukemia and result in dysregulation of the homeobox (HOX) gene cluster, which is critical for persistence of the disease (Bernt et al., 2011; Deshpande et al., 2014). H3K79me1, H3K79me2, and H3K79me3 are thought to play divergent biologic roles in both normal and leukemic contexts, as these marks are associated with active transcription to varying degrees (Barski et al., 2007; Steger et al., 2008) and because efficient tri-methylation of H3K79 requires monoubiquitination of H2BK123 (Schulze et al., 2009). Despite the development of potent chemical probes targeting the DOT1L methyltransferase (Daigle et al., 2011, 2013), it remains unclear how the H3K79 methylation mark is removed and how methylation valence (me1/me2/me3) is established, as no devoted H3K79 demethylase "eraser" has been identified.

In this study, we inducibly tethered the OMLZ domain of the DOT1L subunit AF10 to a synthetic DNA binding domain (ZF-DBD) and used chemical-induced proximity (CIP) (Hathaway et al., 2012; Stanton et al., 2018) to selectively deposit H3K79 methylation at endogenous, un-methylated genes *in vivo* (Figure 1A). Through CIP, we characterize the kinetics

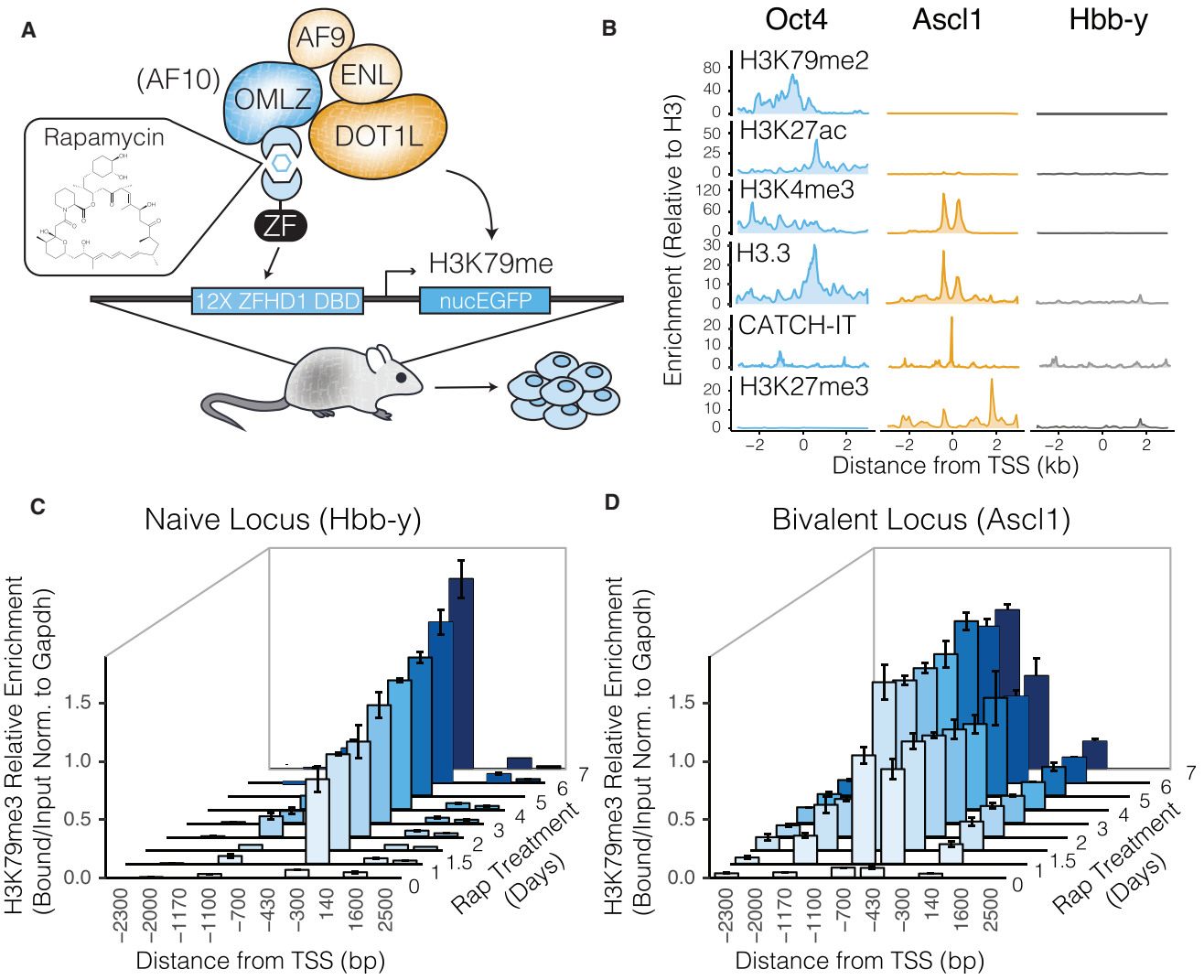

Figure 1. Design and Placement of H3K79me3 in mESC Targeting Lines

(A) CIP cell lines contain a single modified allele harboring two DNA binding arrays upstream of an in-frame EGFP reporter.

(B) Distribution of histone modifications at Hbb-y and Ascl1 in mESCs (Banaszynski et al., 2013; Mikkelsen et al., 2007) compared to the active Oct4 gene.

(C) ChIP analysis of H3K79me3 at the Hbb-y locus over 7 days of rapamycin-mediated recruitment of DOT1L.

(D) ChIP analysis of H3K79me3 at the Ascl1 locus over 7 days of rapamycin-mediated recruitment of DOT1L.

Error bars represent n = 3 experiments.

of mono-, di-, and tri-methylation in real time at diverse chromatin substrates and genomic contexts. We developed a Monte Carlo simulation that couples nucleosome turnover with the system of equations describing processive methylation kinetics. This successfully predicts both the healthy and diseased epigenetic landscapes for a variety of conserved histone marks, including H3K79me. In doing so, we determine that nucleosome turnover is sufficient to establish varied states of methylation. Based on an analysis of the genomic landscapes of worms, flies, and mammals, we propose a conserved general principle for establishing varied epigenetic landscapes in both the presence and absence of active demethylation.

RESULTS

Chemical-Induced Dimerization of DOT1L to Distinct Chromatin Substrates

To define the minimal factors required to orchestrate the methylation states genome-wide, we used chemical-induced proximity of the DOT1L methyltransferase to methylate H3K79 at different genetic loci. We began by generating two distinct, murine embryonic stem cell lines (mESCs) containing an array of DNA binding domains (12xZFHD1) upstream of either the *Ascl1* or the *Hbb-y* transcription start site (TSS) along with an in-frame nuclear EGFP (Figure 1A; Kadoch et al., 2017; Stanton et al., 2017). Two fusion proteins, zinc-finger/FKBP and AF10(OMLZ

domain)/FRB were stably expressed in the mESC recruitment lines by lentiviral transduction to permit rapid deposition of H3K79 methyl marks through small-molecule (rapamycin)-mediated recruitment (Figure 1A). *Ascl1* and *Hbb-y* were specifically targeted as they represent two distinct categories of H3K79me-deficient genomic sites with differing chromatin landscapes. Insertion of the DNA binding arrays at *Hbb-y* represents a "naïve" target locus and enables monitoring of chromatin dynamics independently of other endogenous regulatory factors (e.g., histone marks, transcription factors, remodeling factors, etc.), with minimal exchange of nucleosomes (characterized by levels of H3.3 and CATCH-IT; Banaszynski et al., 2013; Deal et al., 2010; Elsässer et al., 2015; Figure 1B). In contrast, using CIP at a "bivalent" gene (*Ascl1*) allows for monitoring H3K79 dynamics at a poised, highly dynamic locus with histone marks associated with both active and repressed chromatin (compared to a highly transcribed pluripotency factor, such as Oct4; Figure 1B; Braun et al., 2017). An important design consideration of CIP at a "bivalent" gene is that we sought to observe the dynamics of H3K79me by studying the retargeting of DOT1L to natural MLL targets, which occurs aberrantly in mixed lineage leukemia. These two genetic loci served as distinct chromatin substrates, which allowed us to make precise measurements of H3K79me dynamics *in vivo* and in real time. Rapamycin-induced deposition of the H3K79me3 mark was observed at both recruitment sites, yet to varying degrees (Figures 1C and 1D). At the *Hbb-y* locus, a H3K79me3 domain slowly and gradually formed over a period of seven days (Figure 1C), and at *Ascl1*, the maximum enrichment was reached by 2 days (Figure 1D). We confirmed that the placement of the mark is catalytic by inhibition with the DOT1L inhibitor, EPZ-04777 (Figure S1A). However, recruitment of the DOT complex and subsequent placement of the H3K79me3 mark did not result in expression of the EGFP reporter at either locus (Figure S1B). Although it may seem surprising that H3K79me3 is insufficient to activate a heavily H3K4me3-decorated gene in this context, this result does not rule out the possibility that H3K79me is sufficient to initiate transcriptional activation at other loci. Expression of the *Ascl1* transcription factor is heavily reliant on a positive feedback mechanism (Wernig et al., 2007) and, as such, was purposefully knocked out in the mESC reporter line to prevent spontaneous neural lineage differentiation upon induction.

Bivalent and Naive Chromatin Substrates Exhibit Varying Methylation Valency Dynamics

To determine the source of the distinctive H3K79me3 methylation patterns at the *Ascl1* and *Hbb-y* loci, we examined changes of not only tri- but mono- and di-methylation over the course of 7 days. A unique advantage of CIP-mediated kinetic studies is that (-)rapamycin controls allow for more direct comparisons across antibodies, due to the time dependency of such measurements and negligible background. With CIP, we find that, upon 1 day of rapamycin treatment, both *Ascl1* and *Hbb-y* are predominantly mono-methylated (Figure 2A). However, after a week of treatment, the *Ascl1* locus maintains a dominant H3K79me1 state, and at the naive *Hbb-y* locus, H3K79me3 dominates (Figure 2B). By sampling each H3K79 valency state continuously over the course of a week, we find that, at the *Hbb-y* locus, mono-methylation is rapidly acquired and then decreases but that H3K79me3 continually builds over 7 days (Figure 2C). H3K79me2 exhibits a slightly delayed progression, reaching a maximum at 2 days and then similarly decreases (Figure 2C). In contrast, at *Ascl1*, the opposite is observed. H3K79me1, me2, and me3 are each rapidly deposited (with mono-methylation dominating) and appear to reach equilibrium by as early as 12 hr (Figure 2C).

Intrigued by the opposing dynamics of these systems, we compared the respective chromatin immunoprecipitation (ChIP) kinetic profiles to analytical solutions of the system of ordinary differential equations (ODEs) describing the processive-kinetic reactions of methylation:

$$\mathrm{me0} \rightleftharpoons \mathrm{me1} \rightleftharpoons \mathrm{me2} \rightleftharpoons \mathrm{me3}$$

(Figure S1C).

Dominant mono-methylation at equilibrium is consistent with the general solution to the condition in which the forward rate of reaction (k_{on}) is less than the reverse rate of reaction (k_{off}), whereas dominant tri-methylation at equilibrium is consistent with the condition in which $k_{on} > k_{off}$ (Figure 2D). The k_{on} term encompasses methylation rate, whereas the k_{off} term broadly accounts for factors such as cell division, demethylation, and nucleosome exchange. The H3K79me dynamics profiles observed at *Hbb-y* and *Ascl1* are consistent with the predicted methylation states (me1, me2, and me3) of a processive-kinetic model of DOT1L methylation (Figures 2E and 2F). Further, this model successfully predicts previously collected data from yeast (Frederiks et al., 2008; Figure 2G), which measured the global valency states of H3K79, upon induction of yeast dot1 with galactose. Thus, given that the protein levels and rates of recruitment (i.e., concentration of small molecule) are constant in our recruitment system, these findings suggest that H3K79me at *Ascl1* is likely being removed by an active process.

Nucleosome Turnover Model Supports Substrate-Dependent Histone Methylation Dynamics

Because DOT1L is the only known H3K79 methyltransferase and to date no cognate histone demethylase has been identified, we sought to ascertain which regulatory factors may contribute to the differing dynamics observed at the two genetic loci. Similar to actively transcribed genes, bivalent sites, such as *Ascl1*, undergo active nucleosome exchange in order to maintain a poised state at promoters of developmentally important genes (Bernstein et al., 2006; Harikumar and Meshorer, 2015). This is thought to be mediated by the deposition of H3.3, which results in the incorporation of newly synthesized histones (Goldberg et al., 2010). Further, AF9 has been shown to be localized sharply at the TSS of active genes (Figure 3A; Li et al., 2016b), despite the formation of broad H3K79 methylation domains (>20 kb) at these active regions (Soldi et al., 2017). This suggests that a propagation mechanism may contribute to the establishment of the H3K79 landscape. To define the minimal factors required to regulate methylation status, we took an analytical approach to assess the extent to which nucleosome turnover may impact methylation valency. We began by estimating the relative rates

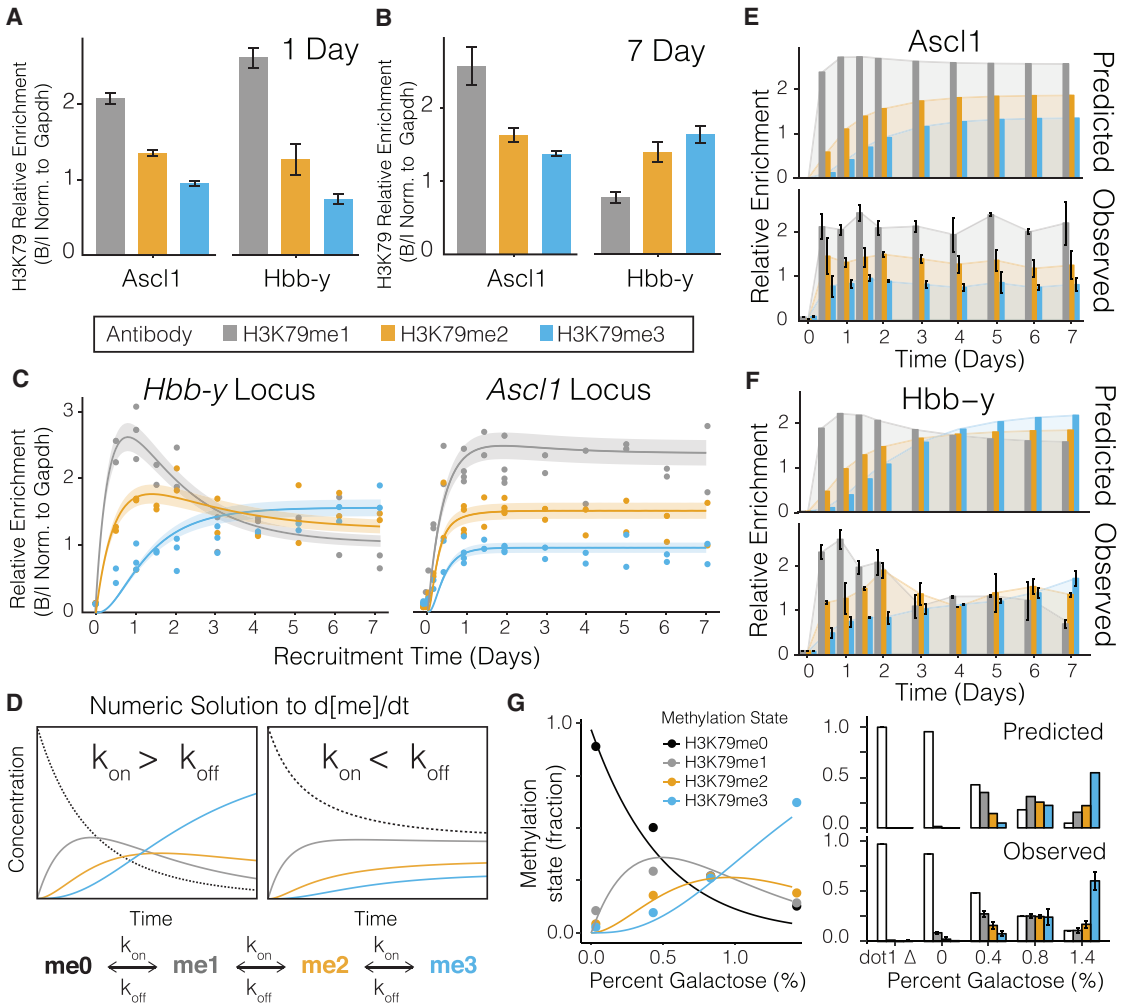

Figure 2. H379me1, me2, and me3 at Various Substrates

(A) ChIP analysis at the recruitment site of Ascl1 and Hbb-y for H3K79me1/me2/me3 following 1 day of Rap treatment.

(B) ChIP analysis at the recruitment site of the Ascl1 and Hbb-y locus for H3K79me1/me2/me3 following 7 days of Rap treatment.

(C) ChIP analysis at the recruitment site of Hbb-y and Ascl1 for H3K79me1/me2/me3 over the course of 7 days (n = 3 experiments). Smoothed lines represent the mathematical chemical kinetic best fit with confidence intervals.

(D) Analytical solutions to the system of ODEs describing processive kinetics for the conditions $k_{on} < k_{off}$ and $k_{on} > k_{off}$.

(E) Observed and predicted H3K79me kinetics at Ascl1.

(F) Observed and predicted H3K79me kinetics at Hbb-y.

(G) Processive methylation kinetics of H3K79me observed by yeast DOT1 (left; Frederiks et al., 2008). Predicted and observed methylation dynamics applying a processive-kinetic model to yeast DOT1 methylation are shown (right).

of nucleosome turnover at *Hbb-y* and *Ascl1* from mESC CATCH-IT data (Banaszynski et al., 2013; Table S1) and observed that the rate of nucleosome exchange at *Ascl1* is roughly 30-fold greater than at *Hbb-y* in mESCs (Figure 1B). Utilizing these respective rates, we developed a Monte Carlo model that simulates the kinetics of a methyltransferase, catalyzing the reaction of an unmodified nucleosome transitioning from me0 → me1 → me2 → me3, based on the probability ($e^{-kt}{}_{on}$) of the reaction occurring within a given time frame (full details in STAR Methods). To the simulation, we added the condition that the modified nucleosome may also move to the right or left within an array at either a high or low turnover rate ($e^{-kt}{}_{right,\ left}$) and *importantly* held the rate of methylation constant (at $k_{on} > k_{off}$; Figure 3B). At the site of nucleation, the results of the simulation of a "low turnover" rate closely resemble the *in vivo* data at the "naïve" locus *Hbb-y* (Figures 3C and 2C). Additionally, minimal methylation domain propagation upstream or downstream of any H3K79 methylation mark is predicted (Figure 3C; Video S1). Conversely, the results of the simulation with high turnover rate (30×) result in local equilibrium concentrations in which me1 > me2 > me3. However, unlike the low turnover rate condition, the profiles propagate upstream and downstream, establishing a dominant mono-methyl domain that spreads bidirectionally over several kb (Figure 3C).

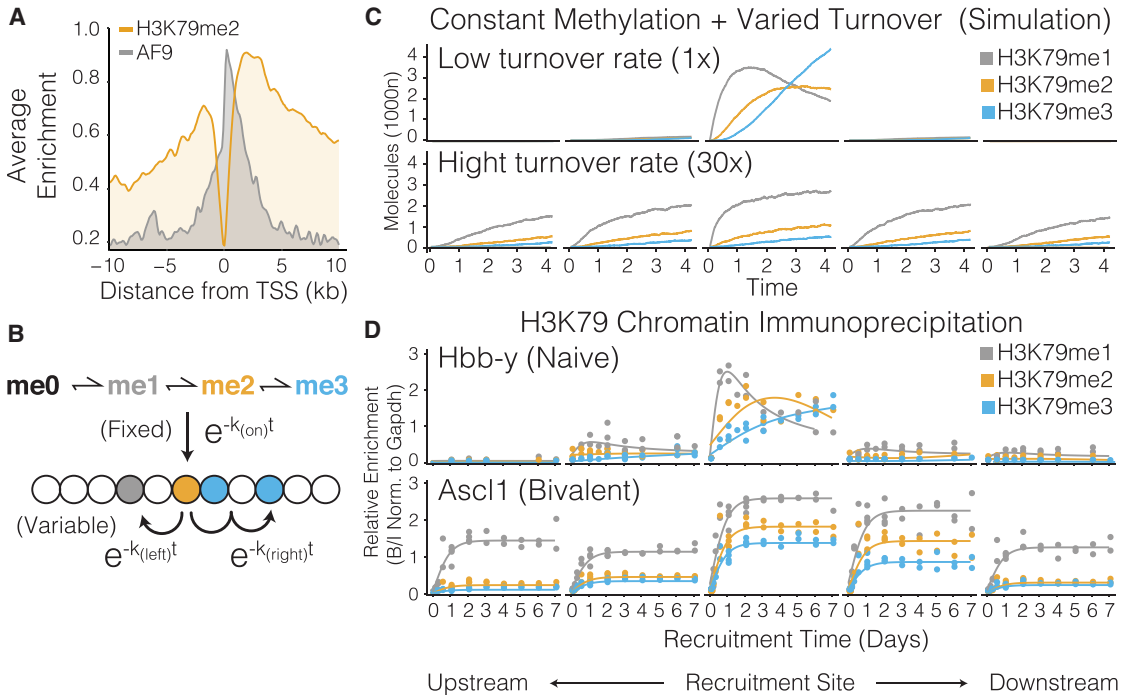

Figure 3. Model of Methylation and Nucleosome Turnover Supports Varied Substrate Dynamics

(A) Distribution of H3K79me2 histone modification and the AF9 subunit in macrophages (Li et al., 2016b; Soldi et al., 2017).

(B) Monte Carlo simulation of methylation and nucleosome turnover considers the chromatin recruitment substrates as a one-dimensional beads-on-a-string.

(C) Results of the Monte Carlo simulations showing −2 to +2 nucleosomes for the conditions of "low nucleosome turnover" (top) and "high nucleosome turnover" (bottom) demonstrate local me3 accumulation or propagation of H3K79me domains, respectively.

(D) ChIP analysis reveals dynamic changes of H3K79me1/me2/me3 chromatin modifications at the Hbb-y locus (top) and propagation of modifications at the Ascl1 locus (bottom). Each data point represents a single immunoprecipitation, at a given treatment point, for n = 3 experiments. Smoothed lines represent the mathematical chemical kinetic best fit.

We then compared the Monte Carlo simulations of "high" and "low" turnover rates to the observed CIP-dependent levels of H3K79me1/me2/me3, upstream and downstream of the TSS at both *Ascl1* and *Hbb-y*. In doing so, it becomes evident that the *in vivo* methylation dynamics we measured by ChIP recapitulate the predicted methylation profiles obtained from the simulations of high and low nucleosome turnover, respectively (Figure 3D). The variable spreading of methylation and subsequent establishment of dominant H3K79me1 versus H3K79me3 domains likely reflect that a central feature of establishing the distinct methylation states is differential nucleosome turnover, even in the absence of active demethylation. This model is supported by the observation that H3K79me1 levels are highly correlated with genomic regions of active transcription (Deshpande et al., 2014), because highly transcribed genes undergo robust polymerase-driven exchange of nucleosomes. Further, given that narrow AF9 peaks are sharply localized near the TSS of transcribed genes despite the establishment of broad H3K79me domains (Figure 3A; Li et al., 2016b; Sabari et al., 2015), a nucleosome turnover model is favored over oligomerization-based processive propagation (Hathaway et al., 2012; Hodges and Crabtree, 2012). Although these results certainly do not rule out the possibility of an undiscovered H3K79 "eraser" (Kang et al., 2018) or undermine the critical functions of other histone demethylases, our model suggests that nucleosome turnover can be sufficient to establish unique methylation states across a variety of genomic contexts, without invoking enzymatic demethylation.

Nucleosome Turnover Coupled with Demethylation Establishes the Polycomb Methylation Landscape

To assess the robustness of our model when factoring in other chromatin regulatory mechanisms, such as demethylation, we sought to investigate methylation valencies of histone modifications with known demethylases, such as polycomb repressive complexes (PRCs). Chromatin remodeling complexes, such as trithorax group proteins and their mammalian homologs (SWI/SNF), are known to oppose the activity of PRCs through histone remodeling and nucleosome turnover (Clapier and Cairns, 2009; Hodges et al., 2016; Kennison and Tamkun, 1988; Wilson et al., 2010). Much like H3K79 methylation, the varying methylation valencies of H3K27 catalyzed by polycomb complexes are known to play divergent roles in transcription (Ferrari et al., 2014; Juan et al., 2017). Tri-methylation of H3K27 mediates gene silencing (Schuettengruber et al., 2017), and H3K27me1 and H3K27me2 are associated with active transcription (Ferrari et al., 2014). Unlike DOT1L, which is thought to have no dedicated demethylase, the demethylation of H3K27me3 is regulated by the Jmj-C domain-containing proteins UTX/KDM6A and JMJD3 (Agger et al., 2007; De Santa

Please cite this article in press as: Chory et al., Nucleosome Turnover Regulates Histone Methylation Patterns over the Genome, Molecular Cell (2018), https://doi.org/10.1016/j.molcel.2018.10.028

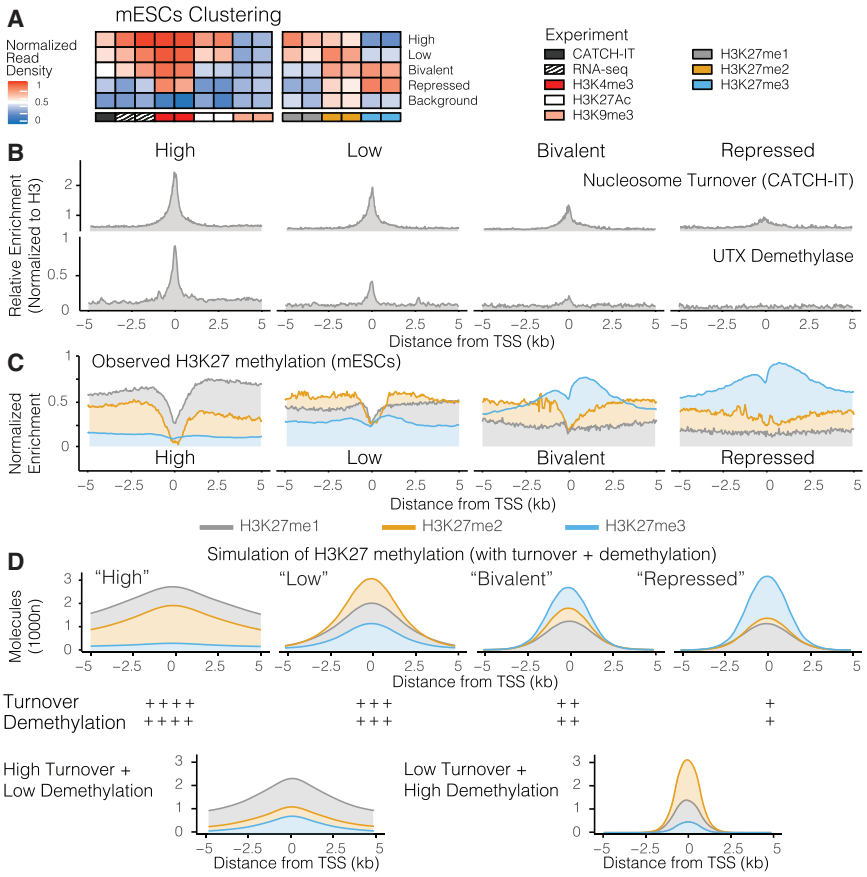

Figure 4. Model of Demethylation and Nucleosome Turnover Predicts Polycomb Methylation State

(A) Average clustering of genomic domains in mESCs cells by k-means, with k = 5.

(B) Average rates of nucleosome turnover and H3K27me2/3 demethylation (UTX) genome-wide at clustered genetic domains.

(C) Meta-analysis of the averaged ChIP-seq signal for H3K27me1/me2/me3 at clustered regions around the TSS of mESCs.

(D) Predicted methylation states over 10 kb from simulation coupling changes in both histone turnover (k_{right} and k_{left}) and demethylation (k_{off}) of H3K27me2/3. "High turnover/low demethylation" and "Low turnover/high demethylation" simulations are shown for comparison.

et al., 2007; Lan et al., 2007; Lee et al., 2007). As studies from Banaszynski et al. (2013) have linked genomic regions of high nucleosome turnover to high localization of H3K27 demethylases in mESCs, we asked to what degree nucleosome turnover rates and/or demethylation play roles in establishing the histone valency states of H3K27me. We began by clustering mESC genes into "high expressing," "low expressing," "bivalent," and "polycomb repressed" bins utilizing a variety of publicly available ChIP sequencing (ChIP-seq) and RNA-seq datasets (Table S1). Although advances have been made to improve the quantitative nature of ChIP sequencing by adding spike-in controls (Orlando et al., 2014), challenges remain to make direct, quantitative comparisons across samples with varying antibodies. To address this issue, we developed an analytical approach, in which we term "normalization by genome-wide integration." We began by normalizing the log-transformed average read density of each transcription start site (±10 kb) within each dataset (Figures S2A and S2B). Instead of normalizing to maximum and minimum reads, which results in data skewing from varied antibody background, we normalized the global integral of each dataset to the maximum and minimum bins obtained from the histogram of average read densities, excluding outliers (Figures S2A and S2B). We then used unbiased k-means clustering of all ChIP-seq datasets for each cell type (Table S1) to identify genes that are characteristic of "high," "low," "bivalent," or "repressed" sites (Figures 4A, S2A, and S2B). "High expressing" genes were characterized by average RNA levels, robust levels of H3K4me3 and H3K27Ac, and no H3K27me3 (full details in STAR Methods). "Low expressing" genes were identified similarly, however with less H3K27Ac. "Bivalent" genes were identified by the presence of both H3K27me3 and H3K4me3, and "polycomb repressed" genes were characterized as having only H3K27me3 (Figures 4A and S2B). We also estimated the average rates of both nucleosome turnover and demethylation (characterized by the amount of UTX at the TSS) and observed that high, low, and bivalent genes display progressive reduction of both nucleosome exchange and demethylation of H3K27me3 (Figure 4B). By applying our normalization-by-integration approach genome-wide to H3K27me1/2/3 (Ferrari et al., 2014; Juan et al., 2017), we observe that, at highly expressed genes, mono-methylation of H3K27 dominates, followed by di-methylation (Figure 4C). However, unlike H3K79me, little to none of the tri-methyl K27 mark is observed at these highly active sites. Also differing from H3K79 is that, at lowly expressed genes, the predominant valency of H3K27 is me2, rather than me1, whereas both bivalent and repressed sites are heavily tri-methylated (Figure 4C). In mESCs, the distribution of H3K27me3 domains is also observably narrower than regions of predominant H3K27 mono- or di-methylation.

To account for the presence of active K27 demethylation in our model, we modified our nucleosome exchange simulation to include varying degrees of *both* turnover and H3K27me3 demethylation by additionally varying the k_{off} term, in accordance with the average rates estimated from the available UTX ChIP-seq and CATCH-IT datasets (Figure 4B). We observe that decreasing rates of both kinetic parameters can broadly account for the H3K27me valency states observed genome-wide in mESCs (Figure 4D). Simultaneously varying these parameters accounts for not only the negligible levels of H3K27me3 observed at "high" expressing genes but also the dominant H3K27me2 domains

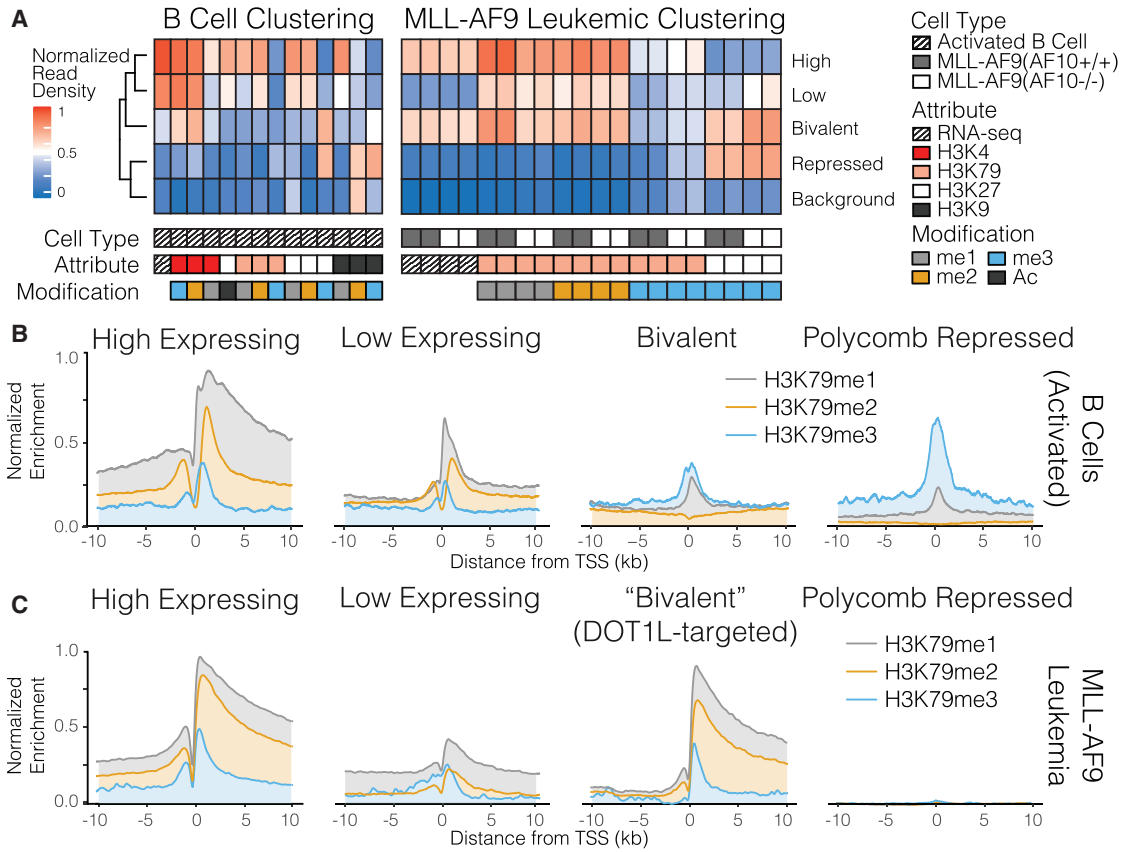

Figure 5. The Nucleosome Turnover Model Predicts Diseased Epigenetic Landscape

(A) Clustering of genomic domains in mature B cells (left; Kieffer-Kwon et al., 2017) and MLL-AF9 leukemias (right; Deshpande et al., 2014) by k-means, with k = 5. Clustering domains were separated into "high expressing," "low expressing," "bivalent," "repressed," and "background" genes.

(B) Meta-analysis of the averaged ChIP-seq signal for H3K79me1/me2/me3 at clustered regions over a ±10 kb genomic region around the transcriptional start sites of mature, activated B cells.

(C) Meta-analysis of the averaged ChIP-seq signal for H3K79me1/me2/me3 and H3K27me3 at four sets of genes over ±10 kb around the TSS of AF10+ MLL-AF9 transformed murine leukemia.

observed at "low" expressing genes (Figure 4D). Therefore, our simulations successfully predict more complex methylation systems genome-wide through the incorporation of additional kinetic factors, such as demethylation. Further, they suggest that, although nucleosome turnover is responsible for establishing the polycomb-mediated valency states of H3K27me, active demethylation of H3K27 primarily results in a binary valency switch and subsequent mutual exclusivity of me1 and me3 domains.

Nucleosome Turnover Model Predicts the DOT1L-Addicted Epigenetic Landscape at MLL Target Genes

We sought to investigate whether modeling nucleosome turnover could predict the fundamental mechanisms driving epigenetically addicted diseases. Fortunately, extensive genome-wide ChIP sequencing has been performed to characterize the phenotypic addiction of MLL-rearranged leukemias to aberrant H3K79me (Bernt et al., 2011; Chen et al., 2015; Deshpande et al., 2014; Erb et al., 2017; Liang et al., 2017; Mueller et al., 2009). Characterizing the relative contributions of nucleosome turnover to methylation is particularly therapeutically relevant to MLL-rearranged leukemias, as DOT1L inhibitors often display delayed anti-proliferative effects despite the rapid loss of H3K79me3 (Daigle et al., 2011, 2013; Yi et al., 2015; Yu et al., 2012). As such, understanding the role of turnover may prove relevant in drugging a variety of histone-methylation-addicted cancers, such as MLL. We began by applying our previous clustering analysis to identify "high," "low," "bivalent," and "repressed" genes in both mature, activated mouse B cells (Kieffer-Kwon et al., 2017) and MLL-AF9 leukemias derived from lineage $^{-}$Sca-1^{+}c-Kit^{+}(LSK) cells from mouse bone marrow (Deshpande et al., 2014; Figures S3A and S3B; Table S1). For healthy B cells, "high," "low," "bivalent," and "polycomb repressed" genes were characterized as described above (full details in STAR Methods; Figures 5A and S3C). In MLL-AF9-transformed leukemias, average RNA levels of each gene and H3K27me3 levels were used to identify each cluster (Figures 5A and S3D). As predicted by the results of our CIP-mediated recruitment experiments and turnover simulations, we observe that, in both active B cells and MLL-AF9-transformed leukemias,

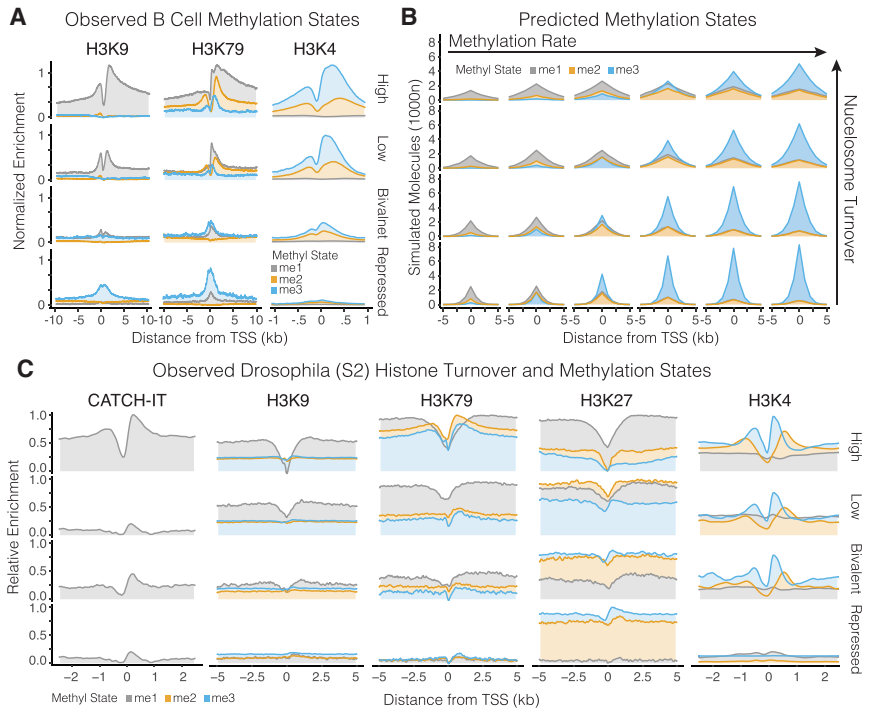

Figure 6. Model of Methylation and Nucleosome Turnover Predicts Conserved Histone Valency States

(A) Clustering of genomic domains in mouse B cells by k-means, with k = 5, showing H3K9 and H3K79 domains over ±10 kb and H3K4 domains over ±1 kb.

(B) Predicted methylation valence states over 5 kb from Monte Carlo simulations coupling changes in both histone turnover and methylation rate.

(C) Relative nucleosome exchange rates (CATCH-IT) and histone methylation valency states "high," "low," "bivalent," and "repressed" genes in *Drosophila* S2 cells (Table S1). CATCH-IT and H3K4 domains are displayed from ±2 kb and H3K9, H3K79, and K3K27 are shown over ±5 kb.

"low expressing" and "high expressing" genomic loci are characterized by H3K79me1 > H3K79me2 > H3K79me3, which propagates over the gene body (Figures 3B and 3C). This is consistent with our nucleosome turnover model (Figure S4A), as transcribed genes exhibit the highest levels of nucleosome turnover in the direction of transcription. We further observe that, in healthy B cells, little H3K79me is observed at either polycomb-repressed sites or bivalent sites, as the presence of H3K27me3 is known to inhibit the binding of AF10 to histones (Chen et al., 2015). The small but sharp H3K79me3 peak observed at polycomb sites is consistent with the "low turnover" model and coincides with repressed genes (Figures 3B and 3C).

Interestingly, in mature B cells, the H3K79 valency states of "bivalent" sites coincide with the methylation profiles of polycomb-repressed genes, akin to the basal methylation state we observed at *Ascl1* in mESCs prior to CIP-mediated recruitment of AF10 (Figure 5B). Conversely, in MLL-AF9 leukemias, the methylation profile at "bivalent" sites starkly resembles that of an actively transcribed gene, despite being heavily decorated with H3K27me3 (Figure 5C). This methylation profile is consistent with the profile at *Ascl1* in mESCs following rapamycin-induced recruitment. Thus, in leukemia, the translocation of DOT subunits with the MLL protein, aberrant recruitment of DOT1L to bivalent sites, and subsequent K79 methylation at these leukemic targets establishes discrete H3K79me1 domains as a result of high levels of nucleosome turnover present at these regions. The H3K79me2 profiles in the MLL-AF4-expressing acute leukemia cell line MV4-11 (Figures S4A and S4B; clustered by H3K27Ac, H3K4me3, H3K27me3, and RNA-seq; Figure S4C), further support the observation that bivalent sites display aberrant methylation propagation of H3K79. Given that, in a normal context, the presence of H3K27me3 would obstruct the binding of AF10 to bivalent genes (Chen et al., 2015), in MLL-AF9 leukemias, our nucleosome turnover model successfully predicts this diseased epigenetic landscape and suggests that these highly turned over sites are likely hyper-sensitive to mis-targeting by the fusion protein. We attribute this sensitivity to the high levels of nucleosome turnover and lack of active enzymatic demethylation, which establish dominant, activating H3K79me1 peaks at these poised genomic regions.

Defining the Minimal Factors Required to Establish the Epigenetic Landscape

Our meta-analysis of H3K79 and H3K27 valency states suggests that nucleosome turnover of marked histones, rather than processive propagation, promotes the spread of these histone modifications around the nucleation sites of methylation. However, the extent to which this model may extend beyond the DOT and polycomb complexes or whether this mechanism is conserved remains unclear. Processive propagation by "reader" proteins is generally thought to establish large heterochromatic domains, such as is observed with the silencing histone mark H3K9me3 (Hathaway et al., 2012; Hodges and Crabtree, 2012; Taverna et al., 2007; Figure 6A). Conversely, the trithorax-mediated *tri-methyl* H3K4 histone mark is associated with active transcription and differs from both H3K9 and H3K79 (Figure 6A) in this regard. However, these methyltransferases are known to have widely varying methylation efficiencies; thus, we sought to examine the extent to which nucleosome turnover may impact the methylation patterns of other classes of methyltransferases. For example, in similar studies, the H3K9 methyltransferase G9a requires more than two hours to fully convert histone peptides to me1, me2, or me3 states (Patnaik et al., 2004), whereas some trithorax group proteins (MLL1-4 and PRDM9) have been shown to fully methylate unmodified H3K4 peptides in as short as 20 min (Li et al., 2016a; Liu et al., 2017). As such, we modified our Monte Carlo model to sample an array of ratios of histone methylation efficiencies to nucleosome turnover rate (Figure 6B) and compared the results of the simulation to a variety of histone methylation marks

genome-wide. We varied both the rate of methylation (1×, 2.5×, 5×, 10×, 15×, and 20×) and the rate of nucleosome turnover (1×, 2×, 5×, and 10×) and simulated the processive methylation of me0 → me1 → me2 → me3 over ±5 kb (Figure 6B). We compared the array of simulated regimes to a variety of methylated histone lysines in mouse B cells (Figure 6A) by applying normalization by integration to each respective mono-, di-, and tri-methyl dataset. We additionally examined whether the histone valence patterning is conserved across species by applying our analysis to genome-wide methylation states of H3K9, H3K4, H3K27, and H3K79 in both *Drosophila* S2 cells (Figures 6C and S5A; Table S1) and early embryonic *C. elegans* (Figure S5B; Table S1). Although in *Drosophila*, the regulation of H3K27me is mediated by highly dynamic regions of chromatin termed polycomb response elements (PREs), we find that the H3K27me valency profiles are consistent with what we observed in mESCs (Figure 6C). In B cells, *Drosophila*, and *C. elegans*, we also observe consistent methylation patterning with varied nucleosome turnover of not only H3K79 but also H3K9 and H3K4 genome-wide (Figures 6A, 6C, and S5C). Further, although the domains of H3K9, H3K79, and H3K27 spread bidirectionally over several kb and are dominated by me1 at highly transcribed genes, sharper peaks are observed for H3K4me. Subsequently, dominant H3K4me3 states fall into the regime in which methylation rate dominates over nucleosome turnover rate (Figure 6B) and is consistent with the measured kinetics of H3K4 methyltransferases (Li et al., 2016a; Liu et al., 2017). As such, a meta-analysis of histone valency states across species, coupled with first-principle kinetic simulations, suggests that processive kinetics of histone methyltransferases, demethylation, and nucleosome turnover define the conserved minimal factors required to predict and model the epigenetic landscape genome-wide.

Transcriptional-Dependent Exchange of Nucleosomes

In the simplest version of our nucleosome turnover model, histone methylation valency at active genes is primarily established by polymerase-dependent exchange of nucleosomes in the direction of the transcriptional unit. If true, upon induction of silenced genes, expression should rapidly result in high levels of mono-methylation of H3K79, followed by di-methylation and tri-methylation. To test this hypothesis, we induced expression of T cell stimulation genes by treating Jurkat cells with phorbol 12-myristate 13-acetate (PMA)/ionomycin and tracked the mono-, di-, and tri-methylation patterns over 12 hr. Specifically, we tracked the methylation patterning at the fas ligand (FASLG) and interleukin-2 (IL-2) genes, which are expressed rapidly in Jurkat cells upon PMA/ionomycin stimulation (Fraser et al., 1991; Kasibhatla et al., 1999). Because these genes are not expressed until T cell activation, there is negligible pre-existing H3K79me. However, we anticipated that, upon PMA/iono stimulation, we would observe rapid K79 methylation, as is observed at transcribed genes.

Time-dependent chromatin immunoprecipitation confirms that, upon T cell stimulation, H3K79me1 is rapidly deposited at both FASLG and IL-2 (Figure 7A). Importantly, we observe that the high fold changes (relative to unstimulated) of mono-methylation at both genes precedes di- and tri-methylation and spreads over the gene body, consistent with our model (Figure S3). This observation supports our prediction that the processive kinetic methylation is opposed by nucleosome propagation, as in the absence of turnover, one would expect to observe a more rapid transition to the tri-methylated state. The correlation between increased transcription and the propagation of the H3K79me marks, is further highlighted by the observation that the methylation spreading is almost entirely downstream of the transcription start site, despite the fact that DOT1L is known to localize primarily to the TSS of active genes (Figure 3A). Although it remains possible that the tri-methylation is being opposed by active demethylation in some contexts, these observed kinetics and distributions support a model upon which local nucleation of a methylation mark and histone turnover in the direction of transcription facilitates the propagation of histones to establish varied methylation valences.

DISCUSSION

Establishing histone methylation states requires an orchestra of readers, writers, and erasers to signal varied biologic outputs (Chi et al., 2010). Although the DOT complex is associated with increased levels of transcription, and translocations of the genes encoding its subunits are strongly implicated in the pathogenesis of mixed lineage leukemias, little is understood about how the varied methylation states of H3K79 are established or removed. Although histone demethylases are often assumed to be the main opposition force to methylation valence, our model presented here suggests that nucleosome turnover is likely a primary contributor to establishing methylation valency genome-wide. Moreover, the correlation between high levels of active transcription and H3K79me1 appears to be simply explained by processive kinetics, which predicts that, in the absence of demethylation and presence of rapid nucleosome turnover, mono-methylation predominates. A nucleosome turnover model supports both the presence of small H3K79me3 peaks in the absence of turnover and may account for the vast H3K79me1 domains that are established at poised H3K4me3 targets in MLL-rearranged leukemias. Whether H3K79me can be removed by demethylases remains possible however; our model provides a rationale supporting the lack of a dedicated demethylase for such a conserved and critical histone regulator. Further, nucleosome turnover and polycomb may regulate the H3K79 methylation state in opposition, with H3K27me3 simply excluding DOT1L from targeting genomic regions in which nucleosomes are being turned over, but not actively transcribed. Not only does our model support the observed genome-wide valency of H3K79 methylation, but when measurable parameters, such as site-specific demethylation and rapid methylation, are added, a nucleosome turnover model explains genome-wide methylation states observed for both activating and repressive histone modifications in both diseased and conserved contexts (Figure 7B). Our model is also strongly supported by recent studies showing that inhibition of histone turnover promotes epigenetic inheritance of repression (Taneja et al., 2017) and that establishment of polycomb domains occurs through nucleation and spreading (Højfeldt et al., 2018; Oksuz et al., 2018). Although the methylation dynamics presented here are simple,

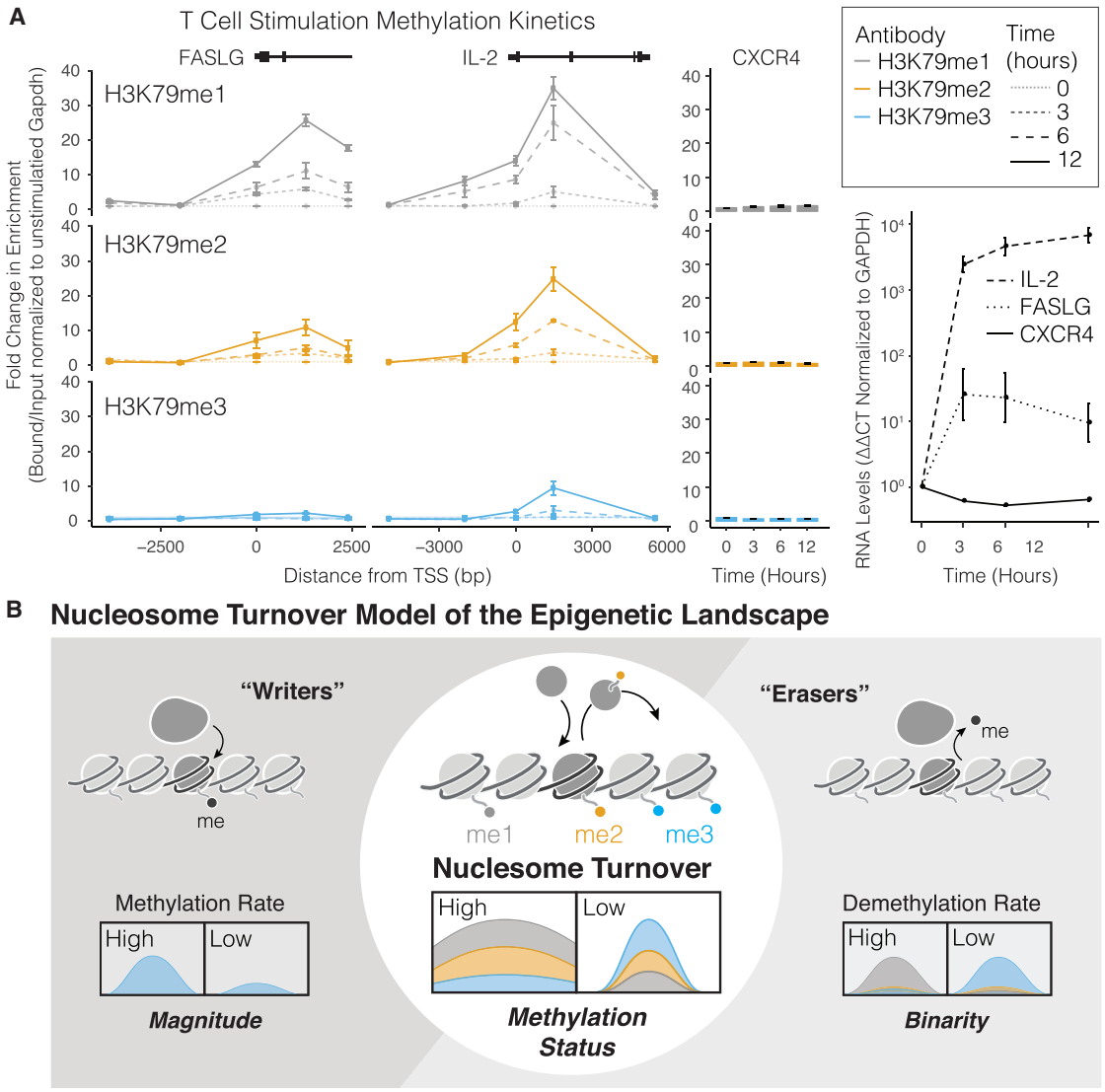

Figure 7. Transcriptional-Dependent Establishment of Methylation State and Model for Nucleosome Turnover Establishment of Histone Methylation Patterns over the Genome

(A) ChIP analysis for H3K79me1, H3K79me2, and H3K79me3 at the FASLG and IL-2 loci following 3 hr, 6 hr, and 12 hr of PMA/ionomycin treatment. qRT-PCR of transcription changes of FASLG and IL-2 and H3K79me1, me, and me3 ChIP at CXCR4 controls.

(B) Nucleosome turnover model of the epigenome.

and alternative processes, such as varied binding affinities and demethylation, make clear contributions, the genomic histone methylation state appears to be characterized by processive first order kinetics, governed by first principles, and largely influenced by the rate of nucleosome turnover.

STAR★METHODS

Detailed methods are provided in the online version of this paper and include the following:

- KEY RESOURCES TABLE
- CONTACT FOR REAGENT AND RESOURCE SHARING
- METHOD DETAILS
  - Construction and Culture of mESC reporter lines
  - Construct Design and Chemical induction of Proximity
  - Chromatin Immunoprecipitation Analysis
  - RT-qPCR Analysis
  - Small-molecule inhibitor
  - ODEs and Monte Carlo Simulations
  - K-Means Clustering of RNA and ChIP-Seq Datasets

SUPPLEMENTAL INFORMATION

Supplemental Information includes five figures, two tables, and one video and can be found with this article online at https://doi.org/10.1016/j.molcel.2018.10.028.

ACKNOWLEDGMENTS

We wish to dedicate this manuscript to the lasting memory of Joseph P. Calarco, who was a brilliant scientist, great friend, and thoughtful colleague and mentor. We thank Dr. James Bradner and Jun Qi for providing EPZ-04777 along with their support and guidance and Dirk Schübeler for providing the targeting Hbb-y cell line. We thank the Crabtree lab, J.G. Kirkland, S.M. Braun, B.Z. Stanton, C.M. Weber, W. Wenderski, C. Hodges, and A.J. Spakowitz for helpful discussions. We would also like to particularly thank the Aiden, Armstrong, Casellas, and Banaszynski labs and the modENCODE collaborators (ENCODE Project Consortium, 2012), whose meticulous generation of ChIP and RNA-seq datasets were invaluable to this study. E.J.C. was supported by an NSF Graduate Research Fellowship and the Ruth L. Kirschstein National Research Service Award (F31 CA203228-02). This study was supported by the Howard Hughes Medical Institute, NIH 5R01CA163915-04, the NIH Javits Neuroscience Investigator Award R37 NS046789-12, the CDMRP Breast Cancer Research Breakthrough Award, and funding from the Simons Foundation Autism Research Initiative.

AUTHOR CONTRIBUTIONS

Conceptualization, E.J.C., J.P.C., N.A.H., O.B., and G.R.C.; Methodology, E.J.C., J.P.C., N.A.H., and O.B.; Investigation, E.J.C. and J.P.C.; Software, E.J.C.; Formal Analysis, E.J.C.; Visualization, E.J.C.; Writing – Original Draft, E.J.C.; Writing – Review & Editing, E.J.C., N.A.H., O.B., and G.R.C.; Funding Acquisition, E.J.C. and G.R.C.; Resources D.S.N.; Supervision, N.A.H., O.B., and G.R.C.

DECLARATION OF INTERESTS

The authors declare no competing interests.

Received: February 26, 2018
Revised: September 4, 2018
Accepted: October 16, 2018
Published: November 21, 2018

REFERENCES

Agger, K., Cloos, P.A.C., Christensen, J., Pasini, D., Rose, S., Rappsilber, J., Issaeva, I., Canaani, E., Salcini, A.E., and Helin, K. (2007). UTX and JMJD3 are histone H3K27 demethylases involved in HOX gene regulation and development. Nature *449*, 731–734.

Banaszynski, L.A., Wen, D., Dewell, S., Whitcomb, S.J., Lin, M., Diaz, N., Elsässer, S.J., Chapgier, A., Goldberg, A.D., Canaani, E., et al. (2013). Hira-dependent histone H3.3 deposition facilitates PRC2 recruitment at developmental loci in ES cells. Cell *155*, 107–120.

Barski, A., Cuddapah, S., Cui, K., Roh, T.-Y., Schones, D.E., Wang, Z., Wei, G., Chepelev, I., and Zhao, K. (2007). High-resolution profiling of histone methylations in the human genome. Cell *129*, 823–837.

Bernstein, B.E., Mikkelsen, T.S., Xie, X., Kamal, M., Huebert, D.J., Cuff, J., Fry, B., Meissner, A., Wernig, M., Plath, K., et al. (2006). A bivalent chromatin structure marks key developmental genes in embryonic stem cells. Cell *125*, 315–326.

Bernt, K.M., Zhu, N., Sinha, A.U., Vempati, S., Faber, J., Krivtsov, A.V., Feng, Z., Punt, N., Daigle, A., Bullinger, L., et al. (2011). MLL-rearranged leukemia is dependent on aberrant H3K79 methylation by DOT1L. Cancer Cell *20*, 66–78.

Braun, S.M.G., Kirkland, J.G., Chory, E.J., Husmann, D., Calarco, J.P., and Crabtree, G.R. (2017). Rapid and reversible epigenome editing by endogenous chromatin regulators. Nat. Commun. *8*, 560.

Chen, S., Yang, Z., Wilkinson, A.W., Deshpande, A.J., Sidoli, S., Krajewski, K., Strahl, B.D., Garcia, B.A., Armstrong, S.A., Patel, D.J., and Gozani, O. (2015). The PZP domain of AF10 senses unmodified H3K27 to regulate DOT1L-mediated methylation of H3K79. Mol. Cell *60*, 319–327.

Chi, P., Allis, C.D., and Wang, G.G. (2010). Covalent histone modifications–miswritten, misinterpreted and mis-erased in human cancers. Nat. Rev. Cancer *10*, 457–469.

Clapier, C.R., and Cairns, B.R. (2009). The biology of chromatin remodeling complexes. Annu. Rev. Biochem. *78*, 273–304.

Daigle, S.R., Olhava, E.J., Therkelsen, C.A., Majer, C.R., Sneeringer, C.J., Song, J., Johnston, L.D., Scott, M.P., Smith, J.J., Xiao, Y., et al. (2011). Selective killing of mixed lineage leukemia cells by a potent small-molecule DOT1L inhibitor. Cancer Cell *20*, 53–65.

Daigle, S.R., Olhava, E.J., Therkelsen, C.A., Basavapathruni, A., Jin, L., Boriack-Sjodin, P.A., Allain, C.J., Klaus, C.R., Raimondi, A., Scott, M.P., et al. (2013). Potent inhibition of DOT1L as treatment of MLL-fusion leukemia. Blood *122*, 1017–1025.

De Santa, F., Totaro, M.G., Prosperini, E., Notarbartolo, S., Testa, G., and Natoli, G. (2007). The histone H3 lysine-27 demethylase Jmjd3 links inflammation to inhibition of polycomb-mediated gene silencing. Cell *130*, 1083–1094.

Deal, R.B., Henikoff, J.G., and Henikoff, S. (2010). Genome-wide kinetics of nucleosome turnover determined by metabolic labeling of histones. Science *328*, 1161–1164.

Deshpande, A.J., Deshpande, A., Sinha, A.U., Chen, L., Chang, J., Cihan, A., Fazio, M., Chen, C.-W., Zhu, N., Koche, R., et al. (2014). AF10 regulates progressive H3K79 methylation and HOX gene expression in diverse AML subtypes. Cancer Cell *26*, 896–908.

Dion, M.F., Kaplan, T., Kim, M., Buratowski, S., Friedman, N., and Rando, O.J. (2007). Dynamics of replication-independent histone turnover in budding yeast. Science *315*, 1405–1408.

Elsässer, S.J., Noh, K.-M., Diaz, N., Allis, C.D., and Banaszynski, L.A. (2015). Histone H3.3 is required for endogenous retroviral element silencing in embryonic stem cells. Nature *522*, 240–244.

ENCODE Project Consortium (2012). An integrated encyclopedia of DNA elements in the human genome. Nature *489*, 57–74.

Erb, M.A., Scott, T.G., Li, B.E., Xie, H., Paulk, J., Seo, H.S., Souza, A., Roberts, J.M., Dastjerdi, S., Buckley, D.L., et al. (2017). Transcription control by the ENL YEATS domain in acute leukaemia. Nature *543*, 270–274.

Ferrari, K.J., Scelfo, A., Jammula, S., Cuomo, A., Barozzi, I., Stützer, A., Fischle, W., Bonaldi, T., and Pasini, D. (2014). Polycomb-dependent H3K27me1 and H3K27me2 regulate active transcription and enhancer fidelity. Mol. Cell *53*, 49–62.

Fraser, J.D., Irving, B.A., Crabtree, G.R., and Weiss, A. (1991). Regulation of interleukin-2 gene enhancer activity by the T cell accessory molecule CD28. Science *251*, 313–316.

Frederiks, F., Tzouros, M., Oudgenoeg, G., van Welsem, T., Fornerod, M., Krijgsveld, J., and van Leeuwen, F. (2008). Nonprocessive methylation by Dot1 leads to functional redundancy of histone H3K79 methylation states. Nat. Struct. Mol. Biol. *15*, 550–557.

Goldberg, A.D., Banaszynski, L.A., Noh, K.-M., Lewis, P.W., Elsaesser, S.J., Stadler, S., Dewell, S., Law, M., Guo, X., Li, X., et al. (2010). Distinct factors control histone variant H3.3 localization at specific genomic regions. Cell *140*, 678–691.

Harikumar, A., and Meshorer, E. (2015). Chromatin remodeling and bivalent histone modifications in embryonic stem cells. EMBO Rep. *16*, 1609–1619.

Hathaway, N.A., Bell, O., Hodges, C., Miller, E.L., Neel, D.S., and Crabtree, G.R. (2012). Dynamics and memory of heterochromatin in living cells. Cell *149*, 1447–1460.

Hodges, C., and Crabtree, G.R. (2012). Dynamics of inherently bounded histone modification domains. Proc. Natl. Acad. Sci. USA *109*, 13296–13301.

Hodges, C., Kirkland, J.G., and Crabtree, G.R. (2016). The many roles of BAF (mSWI/SNF) and PBAF complexes in cancer. Cold Spring Harb. Perspect. Med. *6*, a026930.

Højfeldt, J.W., Laugesen, A., Willumsen, B.M., Damhofer, H., Hedehus, L., Tvardovskiy, A., Mohammad, F., Jensen, O.N., and Helin, K. (2018). Accurate H3K27 methylation can be established de novo by SUZ12-directed PRC2. Nat. Struct. Mol. Biol. *25*, 225–232.

Jenuwein, T., and Allis, C.D. (2001). Translating the histone code. Science *293*, 1074–1080.

Juan, A.H., Wang, S., Ko, K.D., Zare, H., Tsai, P.-F., Feng, X., Vivanco, K.O., Ascoli, A.M., Gutierrez-Cruz, G., Krebs, J., et al. (2017). Roles of H3K27me2 and H3K27me3 examined during fate specification of embryonic stem cells. Cell Rep. *18*, 297.

Kadoch, C., Williams, R.T., Calarco, J.P., Miller, E.L., Weber, C.M., Braun, S.M.G., Pulice, J.L., Chory, E.J., and Crabtree, G.R. (2017). Dynamics of BAF-polycomb complex opposition on heterochromatin in normal and oncogenic states. Nat. Genet. *49*, 213–222.

Kang, J.-Y., Kim, J.-Y., Kim, K.-B., Park, J.W., Cho, H., Hahm, J.Y., Chae, Y.-C., Kim, D., Kook, H., Rhee, S., et al. (2018). KDM2B is a histone H3K79 demethylase and induces transcriptional repression via sirtuin-1-mediated chromatin silencing. FASEB J. *32*, 5737–5750.

Kasibhatla, S., Genestier, L., and Green, D.R. (1999). Regulation of fas-ligand expression during activation-induced cell death in T lymphocytes via nuclear factor kappaB. J. Biol. Chem. *274*, 987–992.

Kennison, J.A., and Tamkun, J.W. (1988). Dosage-dependent modifiers of polycomb and antennapedia mutations in Drosophila. Proc. Natl. Acad. Sci. USA *85*, 8136–8140.

Kieffer-Kwon, K.-R., Nimura, K., Rao, S.S.P., Xu, J., Jung, S., Pekowska, A., Dose, M., Stevens, E., Mathé, E., Dong, P., et al. (2017). Myc regulates chromatin decompaction and nuclear architecture during B cell activation. Mol. Cell *67*, 566–578.e10.

Krivtsov, A.V., and Armstrong, S.A. (2007). MLL translocations, histone modifications and leukaemia stem-cell development. Nat. Rev. Cancer *7*, 823–833.

Lan, F., Bayliss, P.E., Rinn, J.L., Whetstine, J.R., Wang, J.K., Chen, S., Iwase, S., Alpatov, R., Issaeva, I., Canaani, E., et al. (2007). A histone H3 lysine 27 demethylase regulates animal posterior development. Nature *449*, 689–694.

Lee, M.G., Villa, R., Trojer, P., Norman, J., Yan, K.-P., Reinberg, D., Di Croce, L., and Shiekhattar, R. (2007). Demethylation of H3K27 regulates polycomb recruitment and H2A ubiquitination. Science *318*, 447–450.

Li, Y., Wen, H., Xi, Y., Tanaka, K., Wang, H., Peng, D., Ren, Y., Jin, Q., Dent, S.Y.R., Li, W., et al. (2014). AF9 YEATS domain links histone acetylation to DOT1L-mediated H3K79 methylation. Cell *159*, 558–571.

Li, Y., Han, J., Zhang, Y., Cao, F., Liu, Z., Li, S., Wu, J., Hu, C., Wang, Y., Shuai, J., et al. (2016a). Structural basis for activity regulation of MLL family methyltransferases. Nature *530*, 447–452.

Li, Y., Sabari, B.R., Panchenko, T., Wen, H., Zhao, D., Guan, H., Wan, L., Huang, H., Tang, Z., Zhao, Y., et al. (2016b). Molecular coupling of histone crotonylation and active transcription by AF9 YEATS domain. Mol. Cell *62*, 181–193.

Liang, K., Volk, A.G., Haug, J.S., Marshall, S.A., Woodfin, A.R., Bartom, E.T., Gilmore, J.M., Florens, L., Washburn, M.P., Sullivan, K.D., et al. (2017). Therapeutic targeting of MLL degradation pathways in MLL-rearranged leukemia. Cell *168*, 59–72.e13.

Liu, Y., Perez, L., Gill, A.D., Mettry, M., Li, L., Wang, Y., Hooley, R.J., and Zhong, W. (2017). Site-selective sensing of histone methylation enzyme activity via an arrayed supramolecular tandem assay. J. Am. Chem. Soc. *139*, 10964–10967.

Mikkelsen, T.S., Ku, M., Jaffe, D.B., Issac, B., Lieberman, E., Giannoukos, G., Alvarez, P., Brockman, W., Kim, T.-K., Koche, R.P., et al. (2007). Genome-wide maps of chromatin state in pluripotent and lineage-committed cells. Nature *448*, 553–560.

Mueller, D., García-Cuéllar, M.-P., Bach, C., Buhl, S., Maethner, E., and Slany, R.K. (2009). Misguided transcriptional elongation causes mixed lineage leukemia. PLoS Biol. *7*, e1000249.

Nguyen, A.T., and Zhang, Y. (2011). The diverse functions of Dot1 and H3K79 methylation. Genes Dev. *25*, 1345–1358.

Oksuz, O., Narendra, V., Lee, C.-H., Descostes, N., LeRoy, G., Raviram, R., Blumenberg, L., Karch, K., Rocha, P.P., Garcia, B.A., et al. (2018). Capturing the onset of PRC2-mediated repressive domain formation. Mol. Cell *70*, 1149–1162.e5.

Orlando, D.A., Chen, M.W., Brown, V.E., Solanki, S., Choi, Y.J., Olson, E.R., Fritz, C.C., Bradner, J.E., and Guenther, M.G. (2014). Quantitative ChIP-seq normalization reveals global modulation of the epigenome. Cell Rep. *9*, 1163–1170.

Patnaik, D., Chin, H.G., Estève, P.-O., Benner, J., Jacobsen, S.E., and Pradhan, S. (2004). Substrate specificity and kinetic mechanism of mammalian G9a histone H3 methyltransferase. J. Biol. Chem. *279*, 53248–53258.

Radman-Livaja, M., Verzijlbergen, K.F., Weiner, A., van Welsem, T., Friedman, N., Rando, O.J., and van Leeuwen, F. (2011). Patterns and mechanisms of ancestral histone protein inheritance in budding yeast. PLoS Biol. *9*, e1001075.

Sabari, B.R., Tang, Z., Huang, H., Yong-Gonzalez, V., Molina, H., Kong, H.E., Dai, L., Shimada, M., Cross, J.R., Zhao, Y., et al. (2015). Intracellular crotonyl-CoA stimulates transcription through p300-catalyzed histone crotonylation. Mol. Cell *58*, 203–215.

Schmittgen, T.D., and Livak, K.J. (2008). Analyzing real-time PCR data by the comparative C(T) method. Nat. Protoc. *3*, 1101–1108.

Schuettengruber, B., Bourbon, H.-M., Di Croce, L., and Cavalli, G. (2017). Genome regulation by polycomb and trithorax: 70 years and counting. Cell *171*, 34–57.

Schulze, J.M., Jackson, J., Nakanishi, S., Gardner, J.M., Hentrich, T., Haug, J., Johnston, M., Jaspersen, S.L., Kobor, M.S., and Shilatifard, A. (2009). Linking cell cycle to histone modifications: SBF and H2B monoubiquitination machinery and cell-cycle regulation of H3K79 dimethylation. Mol. Cell *35*, 626–641.

Singer, M.S., Kahana, A., Wolf, A.J., Meisinger, L.L., Peterson, S.E., Goggin, C., Mahowald, M., and Gottschling, D.E. (1998). Identification of high-copy disruptors of telomeric silencing in Saccharomyces cerevisiae. Genetics *150*, 613–632.

Soldi, M., Mari, T., Nicosia, L., Musiani, D., Sigismondo, G., Cuomo, A., Pavesi, G., and Bonaldi, T. (2017). Chromatin proteomics reveals novel combinatorial histone modification signatures that mark distinct subpopulations of macrophage enhancers. Nucleic Acids Res. *45*, 12195–12213.

Stanton, B.Z., Hodges, C., Calarco, J.P., Braun, S.M.G., Ku, W.L., Kadoch, C., Zhao, K., and Crabtree, G.R. (2017). Smarca4 ATPase mutations disrupt direct eviction of PRC1 from chromatin. Nat. Genet. *49*, 282–288.

Stanton, B.Z., Chory, E.J., and Crabtree, G.R. (2018). Chemically induced proximity in biology and medicine. Science *359*, eaao5902.

Steger, D.J., Lefterova, M.I., Ying, L., Stonestrom, A.J., Schupp, M., Zhuo, D., Vakoc, A.L., Kim, J.-E., Chen, J., Lazar, M.A., et al. (2008). DOT1L/KMT4 recruitment and H3K79 methylation are ubiquitously coupled with gene transcription in mammalian cells. Mol. Cell. Biol. *28*, 2825–2839.

Taneja, N., Zofall, M., Balachandran, V., Thillainadesan, G., Sugiyama, T., Wheeler, D., Zhou, M., and Grewal, S.I.S. (2017). SNF2 family protein Fft3 suppresses nucleosome turnover to promote epigenetic inheritance and proper replication. Mol. Cell *66*, 50–62.e6.

Taverna, S.D., Li, H., Ruthenburg, A.J., Allis, C.D., and Patel, D.J. (2007). How chromatin-binding modules interpret histone modifications: lessons from professional pocket pickers. Nat. Struct. Mol. Biol. *14*, 1025–1040.

Tiscornia, G., Singer, O., and Verma, I.M. (2006). Production and purification of lentiviral vectors. Nat. Protoc. *1*, 241–245.

Wernig, M., Meissner, A., Foreman, R., Brambrink, T., Ku, M., Hochedlinger, K., Bernstein, B.E., and Jaenisch, R. (2007). In vitro reprogramming of fibroblasts into a pluripotent ES-cell-like state. Nature *448*, 318–324.

Wilson, B.G., Wang, X., Shen, X., McKenna, E.S., Lemieux, M.E., Cho, Y.-J., Koellhoffer, E.C., Pomeroy, S.L., Orkin, S.H., and Roberts, C.W.M. (2010). Epigenetic antagonism between polycomb and SWI/SNF complexes during oncogenic transformation. Cancer Cell *18*, 316–328.

Yi, J.S., Federation, A.J., Qi, J., Dhe-Paganon, S., Hadler, M., Xu, X., St Pierre, R., Varca, A.C., Wu, L., Marineau, J.J., et al. (2015). Structure-guided DOT1L probe optimization by label-free ligand displacement. ACS Chem. Biol. *10*, 667–674.

Yu, W., Chory, E.J., Wernimont, A.K., Tempel, W., Scopton, A., Federation, A., Marineau, J.J., Qi, J., Barsyte-Lovejoy, D., Yi, J., et al. (2012). Catalytic site remodelling of the DOT1L methyltransferase by selective inhibitors. Nat. Commun. *3*, 1288.

STAR★METHODS

KEY RESOURCES TABLE

REAGENT or RESOURCE	SOURCE	IDENTIFIER
Antibodies		
Anti-Histone H3 (mono methyl K79) Antibody	Abcam	Cat#Ab2886; RRID: AB_303388
Anti-Histone H3 (di methyl K79) Antibody	Abcam	Cat#Ab3594; RRID: AB_303937
Anti-Histone H3 (tri methyl K79) Antibody	Abcam	Cat#Ab2621; RRID: AB_303215
Chemicals, Peptides, and Recombinant Proteins		
Rapamycin	Selleckchem	Cat#S1039
Epz04777	Laboratory of Dr. James Brader	N/A
Ionomycin	EMD Milipore	Cat#407952
PMA (Phorbol 12-myristate 13-acetate)	Sigma	Cat#P1585
Experimental Models: Cell Lines		
Jurkat A3 Cells	ATCC	Cat#CRL-2570; RRID: CVCL_1061
mESC Ascl1 CIP line	Braun et al., 2017	N/A
mESC Hbby CIP line	This paper	N/A
Lenti-X^{TM} 293T Cell line	Clonetech	Cat#632180
Oligonucleotides		
Primers for Ascl1 ChIP, See Table S2	Braun et al., 2017	N/A
Primers for Hbb-y ChIP, See Table S2	This paper	N/A
Primers for Faslg ChIP, See Table S2	This paper	N/A
Primers for IL2 ChIP, See Table S2	This paper	N/A
RT Primers, See Table S2	This paper	N/A
Recombinant DNA		
Plasmid: LV EF1a ZFHD1-FKBP-HA (Blast)	This paper	N/A
Plasmid: LV EF1a Frb2x-V5-OMLZ (Puro)	This paper	N/A
Plasmid: psPax2	Tiscornia et al., 2006	Addgene #12260
Plasmid: pMD2.g	Tiscornia et al., 2006	Addgene #12259

CONTACT FOR REAGENT AND RESOURCE SHARING

As Lead Contact, Gerald R. Crabtree is responsible for all reagent and resource requests. Please contact Gerald R. Crabtree at crabtree@stanford.edu with requests and inquiries.

METHOD DETAILS

Construction and Culture of mESC reporter lines

Genome engineering of mouse hhb-y reporter ESCs was achieved through recombinase mediated cassette exchange (RMCE). mESCs containing a targeting site in the *hbb-y* locus with a selection cassette flanked by two inverted *loxP* sites were generously donated by Dirk Schübeler. An insertion cassette was flanked with a *loxP* site upstream of two distinct DNA binding sequence arrays of a minimal IL2 promoter 12xZFHD1 (TAATGATGGGCG) and 5xGal4 (CGGAGTACTGTCCTCCGAG). A nuclear EGFP was inserted downstream of the minimal promoter, followed by a flanking *loxP* site. *Hbb-y* targeting cells were grown under hygromycin for ~10 days prior to RMCE and 4 million mESCs were electroporated with 25 ug of the insertion cassette and 15ug pIC-CRE utilizing the AMAXA nucleofection device and ES nucleofection kit as described by the manufacturer (Program A13). Nucelofected cells were plated on gelatin coated dishes, and single colonies were picked by hand on day 12, briefly trypsonized and plated in a 96 well, gelatin coated plate. Two days after isolating single colonies, the cells were checked for insertion by PCR. Briefly, cells were trypsinized, expanded to create duplicate plates and lysed (Lysis buffer: 0.05% SDS, 0.3 M KCl, 5 mM EDTA, 25 mM TRIS pH 8.3, 1% NP-40, 1% Tween). Lysed cells were digested with 1 mg/mL Proteinase K, heated to 55°C for 1 hour, the Proteinase K was inactivated by heating the 95°C for 10 min, and then analyzed by PCR. *Ascl1* reporter cells were engineered using CRISPR/Cas9 in Stanton et al. (2017) and Kadoch et al. (2017) and generously donated to this study. mES cells were cultured on gelatin coated plates in DMEM media (Life Technologies) containing 7.5% ES-sure FBS (Applied StemCell), 7.5% KnockOut SR (Life Technologies), HEPES buffer

(Life Technologies), Glutamax (Life Technologies), Penicillin-Streptomycin (Life Technologies), 2-mercapto-ethanol (Life Technologies), and MEM-NEAA (Life Technologies), and LIF. Cells were adapted for growth without the use of feeders for all experiments and typically passaged at a density of $3x10^6$cells per 10 cm plate, media was replenished daily, and cells were passaged every 48 hours.

Construct Design and Chemical induction of Proximity

The DNA binding domain (ZFHD1) was fused directly to FKBP12. For DOT1L recruitment, the OMLZ domain of AF10 and nearby flanking region was fused to two tandem repeats of FRB. Lentiviruses were produced in HEK293T Lenti-X cells (Clonetech) via spin-fection with polyethylenimine transfection. HEK cells (Clonetech) were cultured using standard conditions in DMEM media (Life Technologies) containing 10% FBS (Applied StemCell). and Penicillin-Streptomycin (Life Technologies). HEK cells were transfected with PEI (Polysciences Inc., 24765) with lentiviral constructs (Blast ZF-FKBP-HA, Puro 2xFRB-V5-OMLZ) and co-transfected with packaging vectors psPAX2 and pMD2.G as previously described (Tiscornia et al., 2006). 12h after transfection, media was changed, after another 48h, media was collected and supernatant was used to spin-fect mESCs cells in the presence of 10 μg/ml Polybrene (Santa Cruz Biotechnology) at 1000 g for 30min. Stable cell lines were both infected and selected sequentially with 1.5 μg/ml puromycin and 1.5 μg/ml blasticidin beginning 48hr after infection, and maintained under selection for 2-3 passages. Following selection, proximity was induced by addition of rapamycin at 3 nM (final concentration) in all experiments, and media was refreshed daily.

Chromatin Immunoprecipitation Analysis

ChIP experiments were performed as previously described by Hathaway et al. (Hathaway et al., 2012). Briefly, cultured mESCs cells were trypsinized for 5 min, washed with PBS, and fixed for 12 min at room temperature by formaldehyde fixation (final concentration of 1%). Fixation was quenched with 0.125 M glycine and cells were immediately put on ice for 5 min. Crosslinked cells were spun at 1200 × g for 5 min. Nuclei were prepared with 10 mL cell lysis buffer (50 mM HEPES pH 8.0; 140 mM NaCl; 1 mM EDTA; 10% glycerol; 0.5% NP40; 0.25% Triton × 100), then washed in 10 mL rinse buffer (10 mM Tris pH 8.0; 1 mM EDTA; 0.5 mM EGTA; 200 mM NaCl) and pelleted at 1200 g. The chromatin pellets were resuspended in 900 μL shearing buffer (0.1% SDS, 1 mM EDTA pH 8.0, and 10 mM Tris pH 8.0) and sonicated for 12 min using a Covaris focused ultrasonicator at 5% duty cycle, intensity 4, 140 PIP, and 200 cycles per burst. Sonicated chromatin was spun at 10,000 × g for 5 min, and the supernatant was collected, and analyzed for proper shearing on a 1% agarose gel. Immunoprecipitation reactions were set up as follows: Sonicated chromatin was diluted with 0.25 volume of 5 × IP buffer (250 mM HEPES, 1.5 M NaCl, 5 mM EDTA pH 8.0, 5% Triton X-100, 0.5% DOC, and 0.5% SDS) and incubated for 12–16 h at 4°C with 25 μL protein G Dynabeads (Life Technologies) and 5 μg of antibody/IP with overhead rotation. The beads were then washed twice with 1 mL 1 × IP buffer, once with 1 mL DOC buffer (10 mM Tris pH 8; 0.25 M LiCl; 0.5% NP40; 0.5% DOC; 1 mM EDTA), once with 1 mL TE buffer and then eluted in 300 μL elution buffer (1% SDS, 0.1M $NaHCO_3$). Crosslinks were reversed overnight (3hr incubation at 55°C, followed by 65°C overnight), DNA was extracted using Phenol:chloroform (2x), precipitated with isopropanol, and analyzed by qPCR, and normalized to input DNA. Antibodies: H3K79me1 (Abcam #ab2886), H3K79me2 (Abcam #ab3594), H3K79me3 (Abcam #ab2621). For primer distances and sequences, see Table S2.

RT-qPCR Analysis

RNA was extracted from mESCs using Trisure (Bioline) and cDNA was synthesized from 1ug RNA using the SensiFAST SYBR Lo-Rox (Bioline). Delta Samples were run on a QuantStudio 6 Flex system (Life Technologies). $2^{-\Delta\Delta CT}$ *was calculated as described by Livak and Schmittgen* (Schmittgen and Livak, 2008) *where:*

$$-\Delta\Delta CT = (CT_{EGFP} - CT_{Gapdh})_{(-Rap)} - (CT_{GOI} - CT_{EGFP})_{(+Rap)}$$

Primers for RT-qPCR are included in Table S2.

Small-molecule inhibitor

EPZ04777 was partially synthesized by E.J.C. in the laboratory of Dr. James Bradner (Dana Farber Cancer Institute) with the guidance of Dr. Jun Qi and was generously donated to this study. 10 mM stock solutions were prepared in DMSO and stored at −20°C. Serial dilutions of stock solutions were prepared just prior to use.

ODEs and Monte Carlo Simulations

For analytical solutions, k_{on} and k_{off} rates were held constant for each reaction step and solved in MATLAB with numerical solver ode45. For Monte Carlo simulations, methylation reactions and turnover are considered Poisson processes and described by the rates k_{on}/k_{off}, k_{right}/k_{left}, respectively. Poisson processes of H3K79 methylation nucleation site and nucleosome turnover along the lattice are included. Me1, me2, and me3 are nucleated at the recruitment site at a given ration of k_{on} to k_{off} which varies based on methylation/demethylation conditions and turnover of the nucleosomes is equally likely across the lattice and occurs at rates of k_{right}, k_{left}. Each nucleosome is considered as a discrete position within a one-dimensional matrix. The me0 ⇌ me1 ⇌ me2 ⇌ me3 set of methylation reactions occurs exclusively at the center of the lattice, and propagates to the right or the left within the lattice at their respective proportional rates. In the absence of demethylation, nucleosome total loss of methylation (k_-) is set to

zero. All simulations were allowed to evolve under these conditions, for 11 nucleosomes, with no natural boundary elements. For each simulation, 10000 molecules were simulated, with short time steps relative to the fastest possible rate $0.1k_{min}^{-1}$ to give the data plotted in Figures 3C, S2C, and S4A. For Figures 4C and 6B, simulations were ran to equilibrium and iterated across a 1x100 one-dimensional matrix to generate higher-resolution curve predictions.

K-Means Clustering of RNA and ChIP-Seq Datasets

Previously published ChIP-seq and RNA datasets for mature B Cells including: H3K27Ac, H3K4me1, H3K4me3, H3K27me3, and GRO-seq (Kieffer-Kwon et al., 2017) and for MLL-AF9 rearranged leukemias including: H3K27me3, RNA-seq, H3K79me1, H3K79me2, H3K79me3 (Deshpande et al., 2014) were used for deriving gene-class averages following K-means cluster analysis. K-means clustering by using k = 5 was performed on average ChIP-seq/RNA-seq fragment density across ± 10kb from known mouse TSSs, with reads aligned by the original authors. For quantitative ChIP-seq comparisons, average ChIP-seq/RNA-seq fragment density (over ± 10kb) was log10 transformed. To normalize internally to the total density of each histone mark genome wide, average fragment density was normalized to 0 and 1. Upper and lower outliers were ignored in the normalization analysis and were designated by binning all known TSS's into 100 segments, and classifying outlier bins as < $1/1000^{th}$ of the total number of sites (Figure S2A). To make antibody-to-antibody and sample-to-sample comparisons, meta-analysis for the average ChIP-seq signal for H3K79me1, H3K79me1, H3K79me3, and H3K27me3 was normalized internally to each dataset's respective normalization parameters.